Effects of Air Injection on Aerodynamic Performance of a Single-Stage Transonic Axial Compressor

CONG-TRUONG DINH, KWANG-YONG KIM*
Department of Mechanical Engineering
Inha University
253 Yonghyun-Dong, Nam-Gu, Incheon 402-751
REPUBLIC OF KOREA

Abstract: - This paper presents a parametric study of stator air injection on aerodynamic performances of a single-stage transonic axial compressor, NASA Stage 37, using three-dimensional Reynolds-averaged Navier-Stokes equations with the k-ε turbulence model and scalable wall functions. The curvature, location and width of the stator injector and the mass flow rate of air injection were tested to find their effects on the aerodynamic performances, such as total pressure ratio, peak adiabatic efficiency, stall margin and stable range extension. The numerical results for adiabatic efficiency and total pressure ratio were validated with experimental data for smooth casing. The results of parametric study show that the aerodynamic performances of the single-stage transonic axial compressor improve greatly the peak adiabatic efficiency compared to the compressor with smooth casing.

Key-Words: - Single-stage transonic axial compressor, Stator air injection, Reynolds-averaged Navier-Stokes analysis, Total pressure ratio, Adiabatic efficiency, Stall margin, Stable range extension

1 Introduction

In the stator region of a single-stage axial compressor, the flow structure created by the interface between the high speed region near the suction surface and the low speed region near the pressure surface region becomes the source of compressor performance reduction. In order to control this phenomenon, an air injection can be an efficient tool for energizing the flow.

Many experimental and numerical studies have been carried out to investigate the airflow injected in tip clearance of rotor. With reference to the tip injection in rotor domain, Roy et al. [1] studied on the efficiency, stage loading and stable range extension of a low speed axial fan using the tip injection through 6 and 12 nozzles with two injection angles (10° and 30°) located on the rotor casing and upstream of the rotor leading edge. Dobrzynski et al. [2] presented experimentally the effects of steady circumferential and discrete tip injections on the performance of a 1.5-stage low-speed axial compressor, in which the tip injection and bleed increased the operating range and decreased the blockage in the rotor tip region. Kern et al. [3] improved the surge margin of a multi-stage compressor (eight stage HPC at MTU Aero Engines) by using tip injection through 12 injection nozzles equally distributed around the compressor casing. Benhegouga and Ce [4] presented the effects of the injection angle, injection yaw angle, and injector position of tip injection in a range of injection mass flow from 1.25% to 2.5% of smooth casing choking mass flow rate, on the performance of a transonic axial compressor using NASA Rotor 37. Kim et al. [5, 6] reported on parametric study and optimization of a circumferential casing groove combined with tip injection using three design parameters, i.e., the leading edge length, the trailing edge length, and the height of the casing groove in a transonic axial compressor. Through a multi-objective optimization based on these results of parametric study, they found Pareto-optimal designs of the circumferential casing groove with two objective functions, i.e., the stall margin and peak efficiency of a transonic axial compressor. Wang et al. [7] suggested the effects of circumferential coverage of tip injection on aerodynamic performance of a transonic axial compressor using NASA Rotor 37. The results showed that the total pressure ratio, stall margin and stability increased when the circumferential coverage percentage increased from 6% to 87% without change of efficiency, and the maximum performance was achieved at 87% circumferential coverage. Dinh et al. [8] investigated the effects of airflow injection and ejection through a circumferential casing groove in a transonic axial compressor using NASA Rotor 37, on the aerodynamic performances, such as the

total pressure ratio, adiabatic efficiency, stall margin, and stable range extension.

Some experimental researches of NASA-Glenn Low Speed Axial Compressor (LSAC) suggested airflow injection on t he suction surface of stator blades. Culley and Bright [9] investigated the airflow injection from the suction surface of stator blades to reduce the total pressure loss by 25% with airflow injection of 1% mass flow rate of compressor through flow in LSAC. Wundrow et al. [10] suggest an experimental control of flow separation using steady airflow injection at the pressure of 91.7 kPa gauge on the suction surface of stator blades in a low speed axial compressor with increasing the total pressure coefficient. Braunscheidel et al. [11] presented an application of synthetic jets in a low speed axial compressor to reduce the stator flow separation and total pressure loss. The experimental results of Culley and Bright [9], Wundrow et al. [10] and Braunscheidel et al. [11] showed that the injection on the stator suction surface reduced the total pressure loss and the stator flow separation in low speed axial compressor, but without any comment and evaluation on the aerodynamic performances, such as the total pressure ratio, efficiency, stall margin, and stable range extension.

The present work proposes a concept of airflow injection on the stator casing in a single-stage transonic axial compressor using NASA Stage 37, in order to enhance the aerodynamic performances such as total pressure ratio, efficiency, stall margin, and stable range extension of the compressor. These performances were evaluated using three-dimensional (3-D) Reynolds-averaged Navier-Stokes (RANS) equations. Three geometric parameters, i.e., curvature, length and width of the injector located on the stator casing, and an operating parameter, i.e., injection mass flow rate, were selected for the parametric study to find their effects on the aerodynamic performances.

2 Numerical Analysis

2.1 Description of geometry

The single-stage transonic axial compressor studied in this investigation is NASA Stage 37 with 36 rotor blades rotating at a speed of 17185.7 rpm (100% of design speed) and 46 stator blades. The blade airfoil sections of the rotors and stators were designed using multiple circular arcs, the development of the multiple circular arc blade profile is detailed in the NASA TN D-7345 presented by Crouse [12].

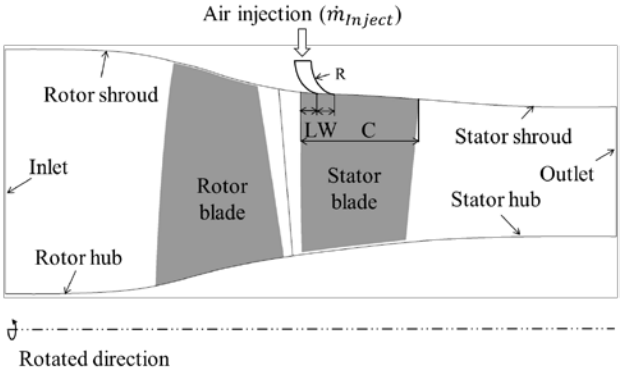

Fig. 1 Geometry of compressor with stator injector.

The design specifications of NASA Stage 37 were reported by Reid and Moore [13]. The values of tip clearances for rotor and stator are 0.04 cm and 0.0762 cm, respectively. And, the total pressure ratio and peak adiabatic efficiency are 2.00 and 84.00%, respectively, at a mass flow rate of 20.74 kg/s. The design stage pressure ratio is 2.05, and the maximum pressure occurs at the mass flow rate about 3% lower than that at the peak adiabatic efficiency and the choking mass flow rate is of 20.93 kg/s at 100% design speed. The references of temperature and pressure are 288.15 K and 101,325 Pa, respectively.

Figure 1 s hows the geometry of the transonic axial compressor (Stage 37) with a stator injector for air injection (one injector per a stator). The airflow injection in the stator domain using the stator injector, energizes the flow in the low speed zone. The stator injector parameters are presented in Fig. 1; the injector width (W) on the shroud was varied from 10% to 20% of the chord length of stator blade at the shroud (C), and the stator injector curvature (R) was also varied in a range, $0.1\ C < R < 0.2\ C$. Leading edge of the injector was located between the stator leading edge to stator trailing edge ($0 < L < C$). A steady airflow was injected through the injector, and the maximum value of the injection mass flow rate was about 2% of the choking mass flow rate of smooth casing. Thus, the injection mass flow rate changed between 1% and 2% of the choking mass flow rate of smooth casing.

2.2 Numerical method

The computation domain in the numerical analysis is comprised of a single passage in a single-stage axial compressor including a rotor, a stator, and an injector. The commercial computational fluid dynamics (CFD) code ANSYS-CFX 15.0 [14] was used for the flow analysis. Blade-Gen and Turbo-Grid were used to create the blade shape and to

generate the computational domain mesh, respectively. Design-Modeler and ICEM-CFD were used to design the stator injection and to generate the mesh, respectively. ANSYS CFX-Pre, CFX-Solver, and CFX-Post were used to define boundary conditions, to solve governing equations, and to post-process the results, respectively.

The hexahedral elements were used to mesh the computational domain. O-type grid was used near the blade's surface, H/J/C/L-type grids were used in other regions of the rotor and stator blocks, and H-type grid was used in the injector block. Grid-dependency test for various performance parameters was performed to find optimum number of grid nodes. The results of the grid-dependency test are introduced in the following section.

The working fluid was considered to be an ideal gas. The average static pressure was set at the stator outlet boundary for steady state simulation. A turbulence intensity of 5% was specified at the rotor inlet boundary. Adiabatic smooth wall condition was used at all wall boundaries. Periodic conditions were used at the side boundaries of the computational domain. The general grid interface (GGI) method was used for the connection between stationary and moving domains. The two-equation k-ε turbulence model with a scalable wall function was used with y+ values for the first nodes near the solid body in a range from 20 to 100.

The convergence criteria proposed by Chen et al. [15] were also used in this work to find the stall point; the inlet mass flow rate variation is less than 0.001 kg/s for 300 steps, the difference between the inlet and outlet mass flow rate is less than 0.3%, and the adiabatic efficiency variation is less than 0.3% per 100 steps.

The performance curves were constructed so that it starts at the choking point and finishes at the last stable convergence point (near-stall point) where the total pressure ratio achieves the maximum value. The performance parameters are total pressure ratio (PR), adiabatic efficiency (η), stall margin (SM), and stable range extension (SRE), which are defined as follows.

$$PR = \frac{P_{t,out}}{P_{t,in}} \tag{1}$$

$$\eta_{peak} = \frac{(\frac{P_{t,out}}{P_{t,in}})^{\frac{\gamma-1}{\gamma}} - 1}{(\frac{T_{t,out}}{T_{t,in}}) - 1} \tag{2}$$

$$SM = \left(\frac{\dot{m}_{peak}}{\dot{m}_{stall}} \times \frac{PR_{stall}}{PR_{peak}} - 1 \right) \times 100\% \tag{3}$$

$$SRE = \left(\frac{(\dot{m}_{\max} - \dot{m}_{stall})_{inject} - (\dot{m}_{\max} - \dot{m}_{stall})_{smooth}}{(\dot{m}_{\max} - \dot{m}_{stall})_{smooth}} \right) \times 100\% \tag{4}$$

where $\dot{m}_{peak}$, $\dot{m}_{stall}$ and $\dot{m}_{\max}$ are mass flow rates at peak efficiency, stall point, and choke condition, respectively. PR_{peak} and PR_{stall} are total pressure ratios at peak efficiency and stall point, respectively. γ, P_t and T_t indicate the specific heat ratio, total pressure, and total temperature, respectively. In the case without airflow injection, the value of SRE was set to be zero.

3 Results and Discussion

A grid dependency test was carried out for the single-stage axial compressor without stator injector with Mesh 1 (total of 336,236 nodes with 208,106 nodes for rotor and 128,130 nodes for stator), Mesh 2 (total of 590,080 nodes with 340,556 nodes for rotor and 249,524 nodes for stator), and Mesh 3 (total of 914,188 nodes with 504,630 nodes for rotor and 409,558 nodes for stator) for the case of a smooth casing. Figure 3 shows the numerical results for the performance curves of the total pressure ratio and adiabatic efficiency for three case tests. Mesh 1 shows 0.54% and 1.23% variations in total pressure ratio and adiabatic efficiency, respectively, compared to those of Mesh 2, but Mesh 3 shows merely 0.07% and 0.18% variations in total pressure ratio and adiabatic efficiency, respectively. Therefore Mesh 2 was determined as the optimum grid. With additional test, it was found that the optimum number of grid nodes for the stator injector combined with 1.5% of smooth casing choking mass flow rate, is 21,840.

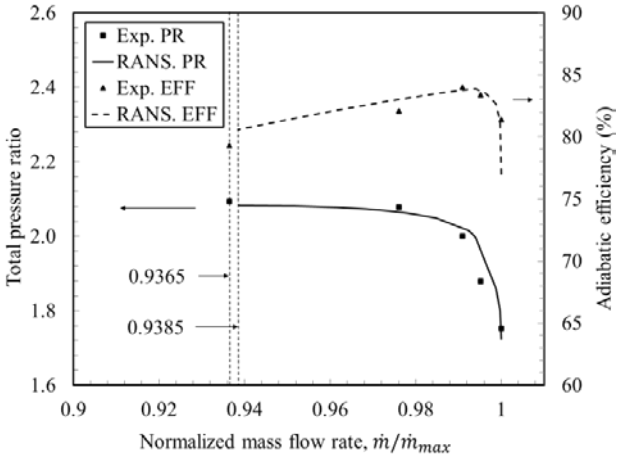

Fig. 2 Validation of computational results with experimental data.

DOI: 10.37394/232022.2021.1.4

Figure 2 shows the numerical performance curves of the total pressure ratio and adiabatic efficiency for the transonic axial compressor without stator injector in comparison with the experimental data reported by Reid and Moore [13]. The numerical results are qualitatively in good agreements with the experimental data. The predicted peak adiabatic efficiency is very close to the measurement, while the predicted total pressure ratio at peak adiabatic efficiency condition is slightly higher than the experimental result. The near-stall point predicted by the RANS analysis is very close to the measurement. The total pressure ratios are slightly under-predicted, but the adiabatic efficiencies are slightly over-predicted compared to the experimental data throughout the whole range of mass flow rate. The predicted stall margin, 9.95%, is very close to the measurement, 10.00%.

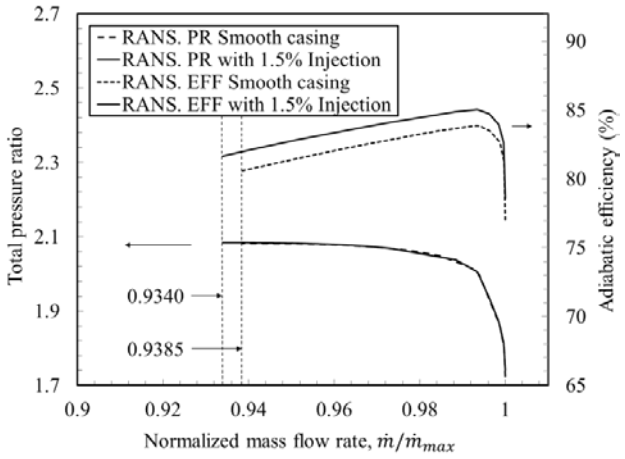

Fig. 3 Comparison between performance curves with and without stator air injection (reference case).

Table 1 Reference dimensionless parameters.

	$\frac{\dot{m}_{Injection}}{\dot{m}_{Choke\_smooth}}$ (%)	L/C (%)	R/C (%)	W/C (%)
Value	1.5	0	20	10

The advantages of using stator injector combined with air injection in a single-stage axial compressor are shown in Fig. 3. Table 1 indicates the values of reference parameters. The results show that the near-stall is significantly delayed using 1.5% air injection (reference case) compared to smooth casing (from normalized mass flow rate of 0.9385 for smooth casing to 0.9340 for reference case), and the peak adiabatic efficiency increases from 83.85% for smooth casing to 85.05% for reference case. The predicted stall margin, 10.63%, is higher than the measurement (9.95%), whereas the total pressure ratio at the peak adiabatic efficiency of the reference case, 2.0042, is slightly smaller than that of the smooth casing. 2.0045. Figure 4 shows the relative Mach number contours at peak efficiency condition on the different planes perpendicular to the axis in the stator domain. The low speed zones observed in Fig. 4(a) for the smooth casing are substantially reduced with 1.5% injection, as shown in Fig. 4(b). This is the main reason for the increase in the peak adiabatic efficiency when using the stator air injection.

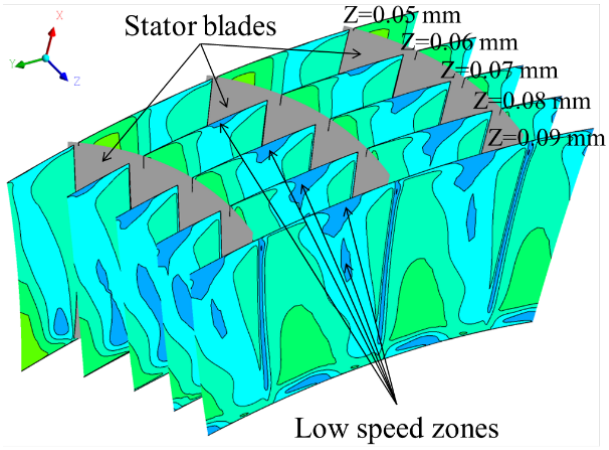

(a) Smooth casing.

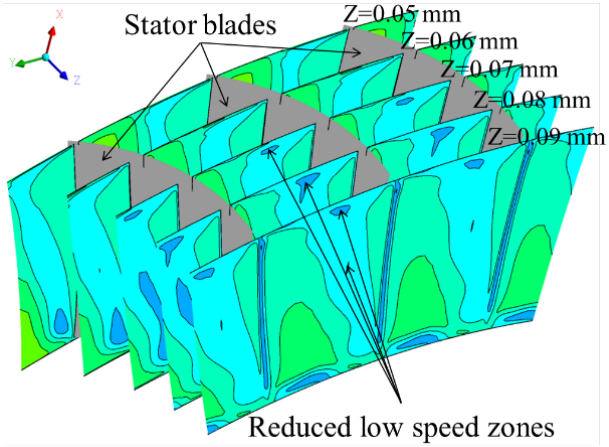

(b) Reference case.

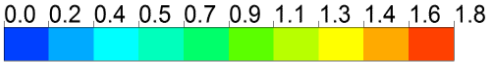

Fig. 4 Relative Mach number contours at peak efficiency condition in stator domain.

Table 2 Ranges of parameters for parametric study.

	$\frac{\dot{m}_{Injection}}{\dot{m}_{Choke\_smooth}}$ (%)	L/C (%)	R/C (%)	W/C (%)
Lower bound	1.0	0	10	10
Upper bound	2.0	100	20	20

The main objective of this work is to study the effects of stator air injection on aerodynamic performances of the single-stage compressor, NASA Stage 37. The location (L), curvature (R) and width (W) of the injector were selected as the geometric parameters and the injection mass flow rate ($\dot{m}_{Injection}$) was selected as the operating parameter for the parametric study. The ranges of these parameters were determined as shown in Table 2.

The results of the parametric study are shown in Figs. 5-8. In the parametric study, the values of parameters that were not being tested were fixed as the reference values (Table 2). Figure 5 shows the effects of injector mass flow rate on different aerodynamic performances of the compressor. The peak adiabatic efficiency and the total pressure ratio at peak efficiency increase with an increase in injection mass flow rate, and show the maximum values at 2.0%, 85.64% and 2.0090, respectively. The maximum stall margin is 10.66% at 1.0% of smooth casing mass flow rate at choking condition and the stall margin reduces with an increase in the mass flow rate. The stable range extension using the injection is highly superior to the smooth casing (0%) and reaches the maximum value of 7.30% at 1.5% of smooth casing mass flow rate at choking condition.

Figure 6 illustrates the effects of injector location on aerodynamic performances of the compressor. The total pressure ratio at peak adiabatic efficiency is larger than that of smooth casing for L/C smaller than 50%, and shows the maximum value of 2.0070 at *L/C*=10%. The relative variation of peak adiabatic efficiency is only 0.03% in the tested range of L/C. The peak adiabatic efficiencies with stator injection are much larger than that of smooth casing; the maximum increment in peak adiabatic efficiency is 1.23%. The stall margin and stable range extension are enhanced remarkably compared to smooth casing; the maximum values are 10.63% and 7.30%, respectively, at L/C=0%.

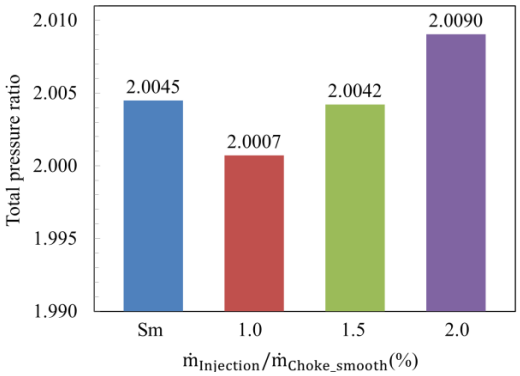

(a) Total pressure ratio.

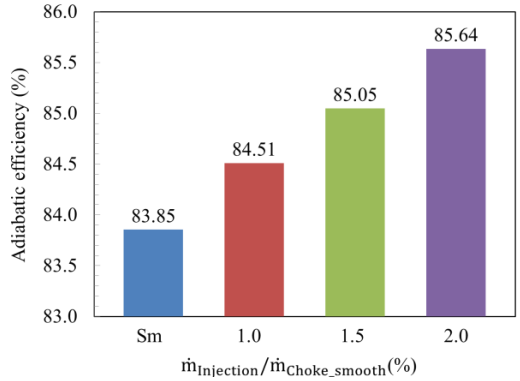

(b) Peak adiabatic efficiency.

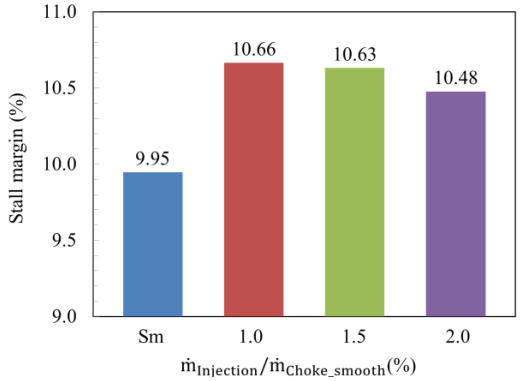

(c) Stall margin.

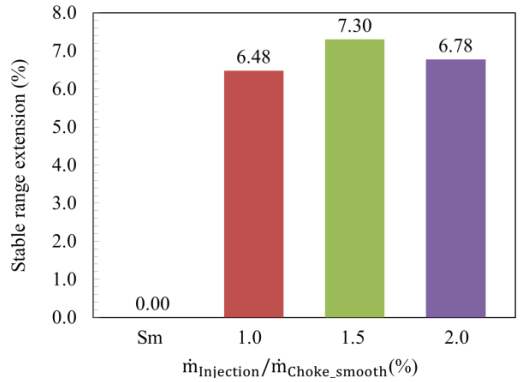

(d) Stable range extension.

Fig. 5 Effects of injection mass flow rate on aerodynamic performances.

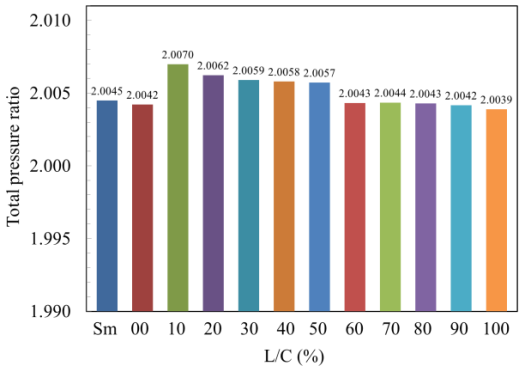

(a) Total pressure ratio.

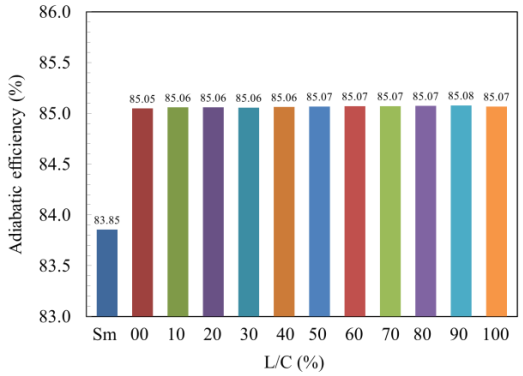

(b) Peak adiabatic efficiency.

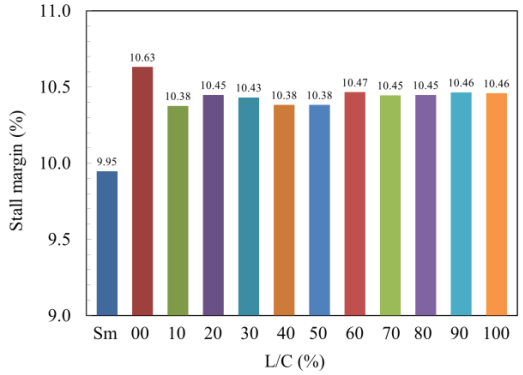

(c) Stall margin.

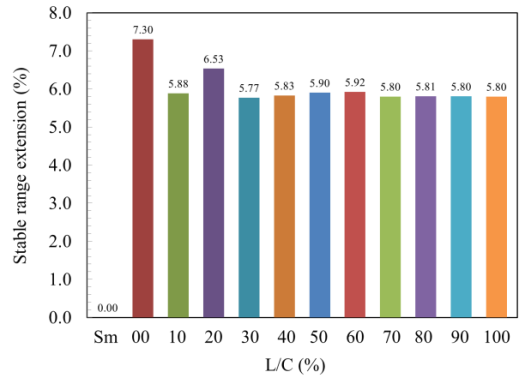

(d) Stable range extension.

Fig. 6 Effects of stator injector location on aerodynamic performances.

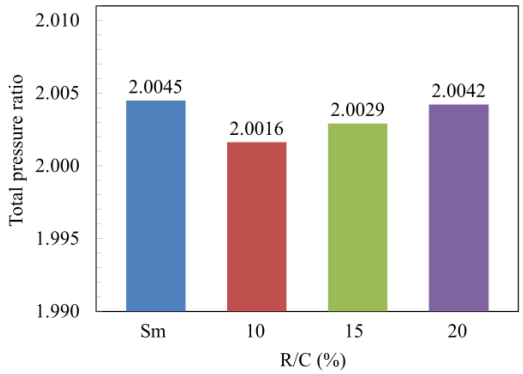

(a) Total pressure ratio.

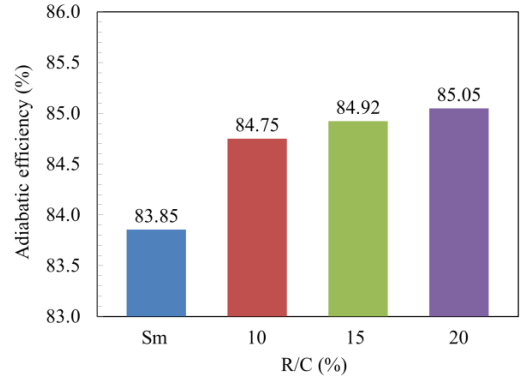

(b) Peak adiabatic efficiency.

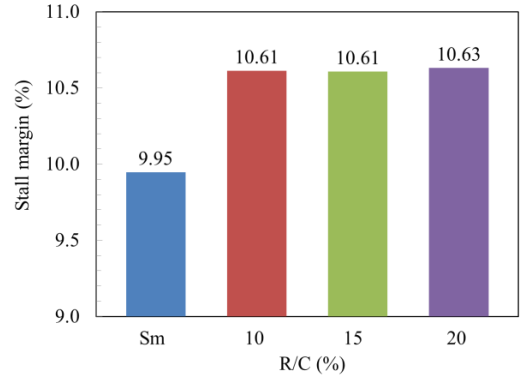

(c) Stall margin.

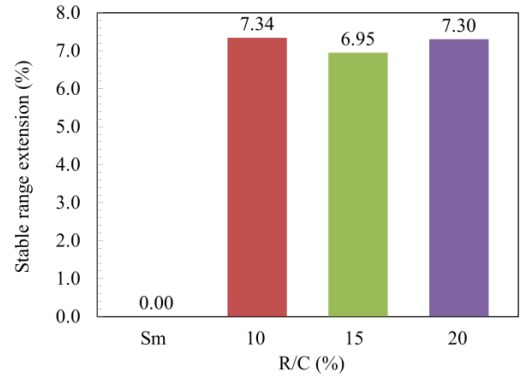

(d) Stable range extension.

Fig. 7 Effects of stator injector curvature on aerodynamic performances.

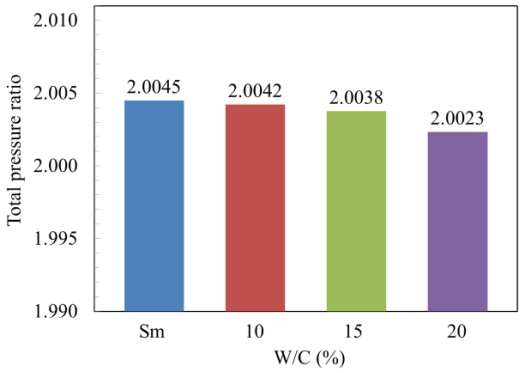

(a) Total pressure ratio.

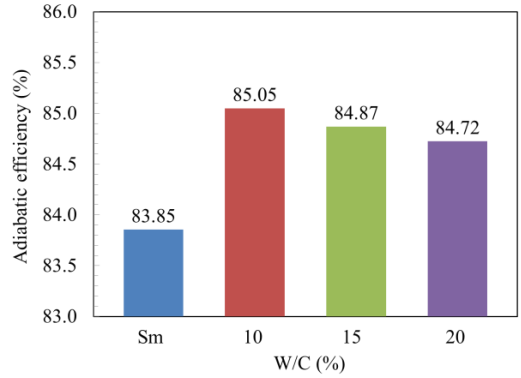

(b) Peak adiabatic efficiency.

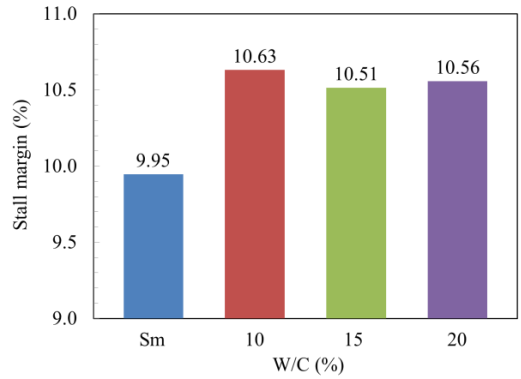

(c) Stall margin.

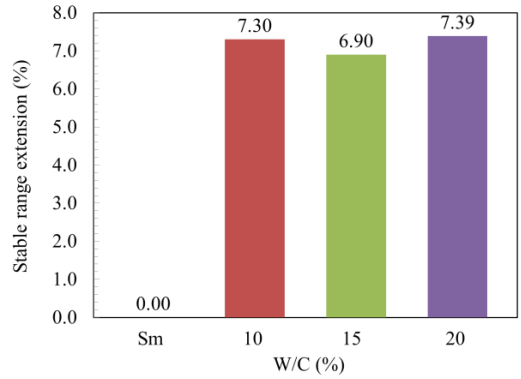

(d) Stable range extension.

Fig. 8 Effects of stator injector width on aerodynamic performances.

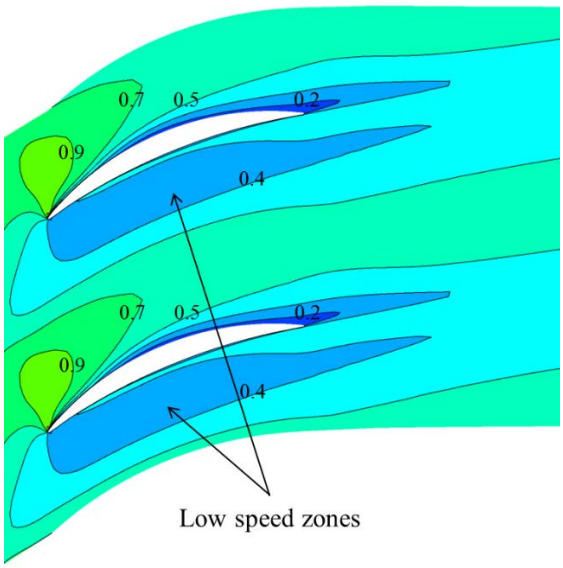

(a) Smooth casing.

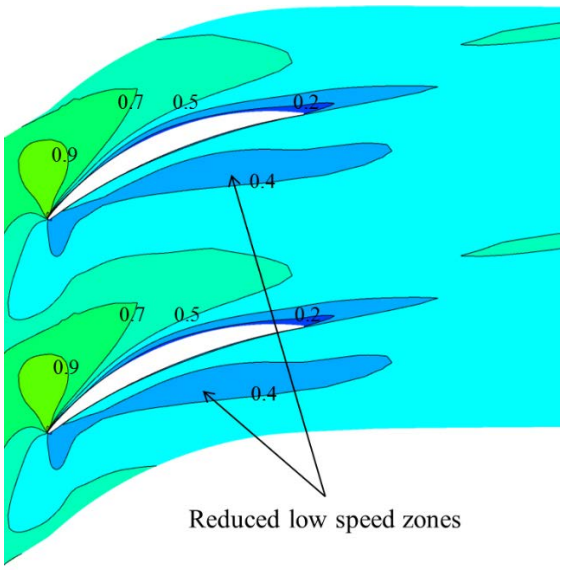

(b) Reference case.

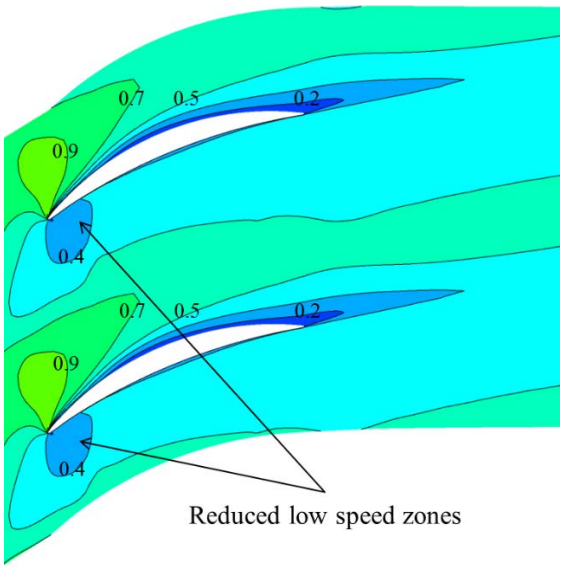

(c) Stator injector length (10%)

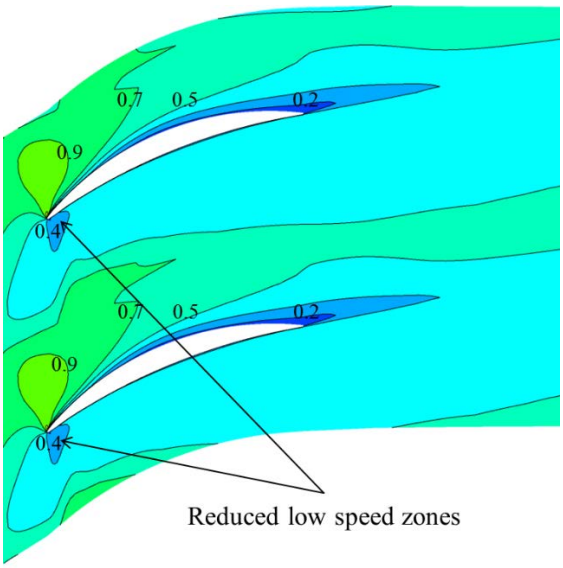

(d) Stator injection (2.0%).

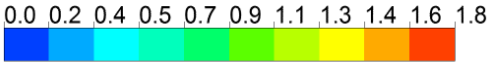

Fig. 9 Relative Mach number contours at 98% span at near-stall condition in stator domain.

The effects of stator injector curvature on aerodynamic performances are shown in Fig. 7. The peak adiabatic efficiency and total pressure ratio at peak adiabatic efficiency increase with an increase in the curvature in a range, 10% < R/C < 20%. However, all the values of total pressure ratio are slightly less than that of smooth casing, while the peak adiabatic efficiency is enhanced largely compared to smooth casing. The maximum values of peak adiabatic efficiency (85.05%) and total pressure ratio at peak adiabatic efficiency (2.0042) are found at R/C=20%. The stall margin and stable range extension are also remarkably improved compared to smooth casing. The maximum stall margin is 10.63% at R/C=20%, and the maximum stable range extension is 7.34% at R/C=10%. However, the maximum variations of stable range extension and stall margin are only 0.39% and 0.02%, respectively.

Figure 8 shows the effects of injector width on aerodynamic performances. The peak adiabatic efficiency and the total pressure ratio at peak efficiency decrease with increase in injector width in a range, 10% < W/C < 20%. The maximum values of peak adiabatic efficiency and total pressure ratio are 85.05% and 2.0042, respectively, at W/C=10%. The stall margin and stable range extension are much larger than those of smooth casing. The maximum stall margin is 10.63% at W/C=10%, while the maximum stable range extension is 7.39% at W/C=20%. The differences between the maximum and minimum values of stable range extension and stall margin are only 0.49% and 0.12%, respectively.

Figure 9 shows relative Mach number contours at 98% span at near-stall condition in the stator domain for smooth casing and the cases of maximum peak adiabatic efficiency using stator injection. The low speed zones observed in the Fig. 9(a) for smooth casing are clearly reduced using stator injection as shown in Figs. 16(b-d). The low speed zones shown in the Fig. 16(b) disappear in Figs. 16(c) and 16(d), due to the increases in total pressure ratio and peak adiabatic efficiency.

4 Conclusion

A single-stage transonic axial compressor, NASA stage 37, with stator injector was investigated numerically using 3-D RANS equations. The numerical results for total pressure ratio and adiabatic efficiency were validated as compared to experimental data for the compressor with smooth casing. A parametric study was performed to find the effects of geometric and operating parameters on the aerodynamic performances of the compressor with stator injection. The curvature, width and location of the stator injector were selected as the geometric parameters, and the mass flow rate of injection was selected as the operating parameter. The results show that the injection mass flow rate has significant influence on the total pressure ratio and adiabatic efficiency. The maximum values of the total pressure ratio and peak adiabatic efficiency were 2.0090 and 85.64%, respectively, at 2.0% mass flow rate of injection, and the maximum stable range extension was 7.39% at L/C=20%. These values indicate largely improved performance of the compressor as compared to smooth casing, of which total pressure ratio, peak adiabatic efficiency, and stable range extension are 2.0045, 83.85% and 0%, respectively. However, the stall margin was not improved remarkably by stator injection; the maximum stall margin was 10.66% at 1.0% mass flow rate of injection, while the stall margin for smooth casing was 9.95%. It is concluded that the aerodynamic performances of the single-stage axial compressor were significantly augmented by using stator injection as compared to the compressor with smooth casing.

References:

[1] B. Roy, M. Chouhan and K. V. Kaundinya, Experimental study of boundary layer control through tip injection on straight and swept

compressor blades, *Proceedings of GT2005, ASME Turbo Expo 2005: Power for Land, Sea and Air*, June 6-9, 2005, Reno-Tahoe, Nevada, USA, GT2005-68304.

[2] B. Dobrzynski, H. Saathoff and G. Kosyna, Active flow control in a single-stage axial compressor using tip injection and endwall boundary layer removal, *Proceedings of ASME Turbo Expo 2008: Power for Land, Sea and Air*, June 9-13, 2008, Berlin, Germany, GT2008-50214.

[3] M. Kern, W. Horn, S.-J. Hiller and S. Staudacher, Effects of tip injection on the performance of a m ulti-stage high-pressure compressor, *CEAS Aeronaut J*, Vol. 2, 2011, pp. 99–110.

[4] I. Benhegouga, and Y. Ce, Steady Air Injection Flow Control Parameters in a Transonic Axial Compressor, *Research Journal of Applied Sciences, Engineering and Technology*, Vol. 5(4), 2013, pp. 1441-1448.

[5] D. W. Kim, J. H. Kim, and K.Y. Kim, Aerodynamic Performance of an Axial Compressor with a Casing Groove Combined with Injection, *Transactions of the Canadian Society for Mechanical Engineering*, Vol. 37 (3), 2013, pp. 283-292.

[6] J. H. Kim, D. W. Kim, and K. Y. Kim, Aerodynamic optimization of a transonic axial compressor with a casing groove combined with tip injection, *Proceedings of The Institution of Mechanical Engineers, Part A: Journal of Power and Energy*, Vol. 227 (8), 2013, pp. 869-884.

[7] W. Wang, W. Chu, H. Zhang, and Y. Wu, Numerical Investigation on the Effects of Circumferential Coverage of Injection in a Transonic Compressor with Discrete Tip Injection, *Proceeding of ASME Turbo Expo 2014: Turbine Technical Conference and Exposition*, Dusseldorf, Germany, GT2014-25420, June 16-20, 2014.

[8] C. T. Dinh, M. W. Heo and K. Y. Kim, Aerodynamic performance of transonic axial compressor with a casing groove combined with blade tip injection and ejection, *Aerospace Science and Technology*, Vol. 46, 2015, pp. 176-187.

[9] D. E. Culley, M. M. Bright, P. S. Prahst and A. J. Strazisar, Active Flow Separation Control of a Stator Vane Using Surface Injection in a Multistage Compressor Experiment, *NASA/TM—2003-212356, Turbo Expo 2003*, Atlanta, Georgia, United States, GT2003–38863, June 16–19, 2003.

[10] D. W. Wundrow, E. P. Braunscheidel, D. E. Culley, and M. M. Bright, Separation Control in a Mu ltistage Compressor Using Impulsive Surface Injection, *NASA/TM—2006-214361*.

[11] E. P. Braunscheidel, D. E. Culley and K. B. M. Q. Zaman, Application of Synthetic Jets to Reduce Stator Flow Separation in a Low Speed Axial Compressor, *NASA/TM—2008-215145, 46th Aerospace Science Meeting and Exhibit*, Reno, Nevada, United State, AIAA–2008–0602, January 7–10, 2008.

[12] J. E. Crouse, Computer program for definition of transonic axial-flow compressor blade rows, *NASA Technical Note*, NASA TN D-7345, February 1974.

[13] Lonnie Reid and Royce D. Moore, Design and Overall Performance of Four Highly Loaded, High-Speed Inlet Stages for an Advanced High-Pressure-Ratio Core Compressor, *NASA Technical Paper 1337*, October 1978.

[14] ANSYS CFX-15.0.0, *ANSYS CFX-Solver Theory Guide*, ANSYS Inc., 2013.

[15] H. Chen, X. D. Huang, and S. Fu, CFD Investigation on Stall Mechanisms and Casing Treatment of a Transonic Compressor, *In: 42nd AIAA/ASME/SAE/ASEE Joint Propulsion Conference & Exhibit*, Sacramento, USA. AIAA-2006-479, 2006.